Optimal Design of a Redundantly Actuated 4-Legged Six Degree of Freedom Parallel Manipulator Using Composite Design Index

Byung-Ju Yi* and Whee-Kuk Kim**

(Received March 2, 1994)

This work attempts to develop a procedure for the optimal design of a redundantly actuated six degree of freedom parallel manipulator. A concept of composite design index is developed to deal with multi-criteria based design in a systematic manner, and this index is employed to obtain a set of optimal dimensions for this manipulator. Two different designs are investigated, and they are compared in terms of their local characteristics. Finally, the fault-tolerant capability afforded by redundant actuation is evaluated in terms of partial actuator failures.

Key Words: Composite Design Index, Redundant Actuation, Multi-Criteria Based Design, Parallel Manipulator, Fault Tolerant

1. Introduction

Parallel closed-chain mechanisms have been implemented often in robot design. They have some attractive advantages when compared to the more commonly used serial chain mechanism. Structurally, parallel mechanisms possess several individual load paths to the ground. Consequently, they have greater geometric complexity which in turn enhances their ability to deliver higher payload capacity, higher stiffness, etc.

The Stewart Platform is one example of parallel connection robot manipulators, which have six degrees of freedom(DOF), six legs, and six linear actuators. Stewart(1965) initially suggested using this mechanism as an aircraft simulator motion base. Hunt(1983) among others, suggested its use as a manipulator and addressed some alternative mechanical designs for this mechanism. Freeman and Tesar(1988) presented a complete kinematic and dynamic modeling method of this kinds of mechanism. Many researchers have designed this kind of mechanism for laboratory implementation.(Han et al., 1989; Kim, 1989; Kurz and Hayward, 1990) Ma and Ageles(1991) discussed design issues with respect to architectural singularity.

The abundance of potential input locations in structurally parallel closed-chain mechanisms allows the implementation of redundant actuation (i.e., extra input drivers), which may be utilized for optimal load distribution and beneficial internal load generation (Kumar and Gardner, 1990; Kurz and Hayward, 1990; Meyer and Angeles, 1989; Yi et al., 1992). Redundancy in the actuation subsystem also admits fault tolerance capability when some of the actuators in the system fail(Sreevijayan, 1992; Ting et.al., 1993; Wu et.al., 1991). In this work, we investigate another type of six DOF manipulator which consists of four legs, where each leg contains an active gimbal joint, a passive revolute joint, and a passive ball joint. Figure 1 is a schematic of this mechanism. The special feature of this mechanism is redundant actuation, which provides the system with internal load adjustment, and fault tolerance in case of any actuator failure. Also, since this mechanism has less legs than the typical six-legged Stewart Platform minipulator does, it has more workspace and better dexterity. In this paper, we investigate the design problem of this mechanism. Specifi-

* Department of Mechanical Engineering, Korea Institute of Technology and Education, Cheon An P. O. Box 55, Chung Nam, Korea 330-600

** Department of Control and Instrumentation Engineering, Korea University, Seo-Chang Dong, Chochiwon Eup, Yonki Kun, Chung Nam, Korea

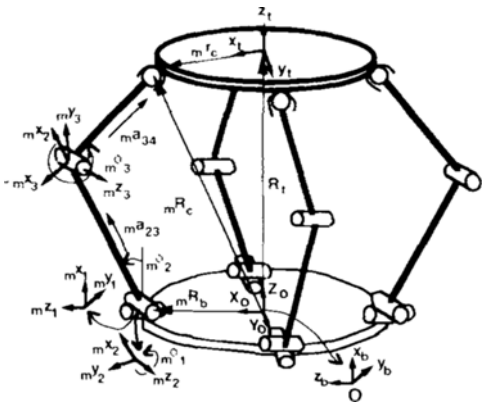

Fig. 1 4-Legged 6 DOF parallel manipulator

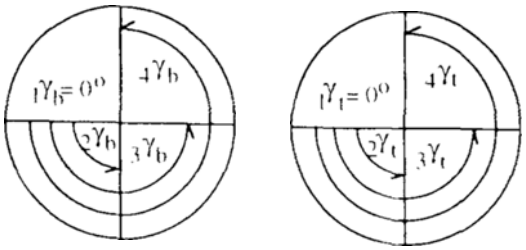

(a) Base plate (b) Top plate

Fig. 2 Displacement angles

cally, the ultimate goal of this work is a dimensional synthesis of this mechanism.

Several geometric and kinematic criteria have been developed for the purposes of enhanced operation (Klein and Blaho, 1987; Kumar and Gardner, 1990) and optimal design(Gosselin and Angeles, 1987; Kurz and Hayward, 1992; Parden and Sastry, 1989; Yi et al., 1992). However, a single criterion based design does not provide sufficient control on the range of the design parameters involved. Therefore, multi-criteria based design have been proposed(Kurz and Hayward, 1992). However, the previous multi-criteria methods have yet to provide any systematic design procedure. In this paper, a concept of composite design index is proposed to systematically deal with multi-criteria based design.

2. Geometric Description

The six DOF mechanism shown in Fig. 1 has four legs which connect the base and the top plates in parallel. The subscript 'm' denotes the leg. Each leg consists of two parallel actuated joints at the base, one passive revolute joint in the middle of the leg, and one passive ball and socket joint at the top plate. For simplicity in design, the four legs are distributed symmetrically. Therefore, the locations of each gimbal mechanism on the base plate are arranged in a 90° increment. These displacement angles are denoted as ${}_1\gamma_b=0°$, ${}_2\gamma_b=90°$, ${}_3\gamma_b=180°$ and ${}_4\gamma_b=270°$, respectively. The locations of the ball and socket joints on the top plate are also arranged in a similar fashion as ${}_1\gamma_t=0°$, ${}_2\gamma_t=0°$, ${}_3\gamma_t=0°$ and ${}_4\gamma_t=270°$, respecitively. Figure 2 illustrates these displacement angles.

Two coordinate systems are defined to describe the relative position of the moving platform with respect to the base plate. The coordinate system (X_0, Y_0, Z_0) fixed on the base plate is considered the global reference frame. The vector from the origin to the position of the gimbal joint of the first leg is defined as the global X_0 vector, and the vector perpendicular to the base plate is defined as the global Z_0 vector. Another coordinate system is attached to the moving plate. The coordinate system (x_t, y_t, z_t) is defined similarly as shown in Fig. 1.

The radii, r and R, of the top and base plates are the distances from the origin of the moving coordinates system to the center of the ball and socket joint, and from the origin of the global reference coordinate system to the center of the gimbal joints, respectively. ${}_mL_1$ and ${}_mL_2$ represent the lengths of the lower link and the upper link, respectively.

3. Design Specifications and Design Parameters

Manipulator specifications include workspace, actuator type, payload, accuracy, weight, nominal velocity, etc. The specifications will vary according to the application. Here, our goal is to design a force reflecting manual controller mechanism. The followings are the specifications for this particular application :

Output Range : $-45° \leq \mu_1, \mu_2 \leq 45°$,
$-90° \leq \mu_3 \leq 90°$ (μ_1, μ_2, μ_3 : Euler angles)
Actuator Type : Four 2-DOF Gimbal Mechanisms with Dual DC Motors
Accuracy : 0.001 inch
Total Weight/Payload : 150 lbs.(max.)/50 lbs
Nominal Velocity : $V_0 = 40$ inch/sec,
$\omega_0 = 6$ rad/sec
Maximum Height : 30 inch (max. for manual controlling mechanism design (Parsons, 1985))

Several parameters are considered in the design of this mechanism. Symmetry of this mechanism reduces the number of design parameters. We set all twist angles (α_{01}^m, α_{12}^m, α_{23}^m : m = 1 – 4) to 90°. The twist angle α_{ij}^m is defined as $\cos^{-1}({}_m\hat{z}_i \cdot {}_m\hat{z}_j)$. Therefore, only four design parameters, r, R, L_1 and L_2, remain. As noted in the design specifications, the size of the gimbal mechanism should not exceed the size of R and the maximum height of the manipulator should not exceed the limit of 30 inches.

4. Kinematics

4.1 Reverse position analysis

From reverse position analysis, the system joint information can be obtained for a specified operational position. First of all, all the vectors describing the positions of the mechanism will be obtained. The position vectors ${}_mr_c$ and ${}_mR_b$ (shown in Fig. 1) are the vectors from the origin of the local upper platform reference coordinate to the ball and socket joint, and from the origin of the global lower platform reference coordinate to the gimbal joint, respectively. They are written as

$$ {}_1r_c = (r, 0, 0)^T,\ {}_2r_c = (0, r, 0)^T, $$
$$ {}_3r_c = (-r, 0, 0)^T,\ {}_4r_c = (0, -r, 0)^T \quad (1) $$

and

$$ {}_1R_b = (R, 0, 0)^T,\ {}_2R_b = (0, R, 0)^T, $$
$$ {}_3R_b = (-R, 0, 0)^T,\ {}_4R_b = (0, -R, 0)^T. \quad (2) $$

The position vector of the ball and socket joint is denoted as

$$ {}_mR_c = R_t + [R_b^t]\,{}_mr_c^{(t)} = R_t + {}_mL_1 \cdot {}_ma_{23} + {}_mL_2 \cdot {}_ma_{34}, \text{ for } m = 1, 2, 3, 4 \quad (3) $$

where $[R_b^t]$ represents the trasformation matrix of the top platform with respect to the lower platform, and the local unit vectors, ${}_ma_{23}$ and ${}_ma_{34}$ directed along the link 1 and 2, respectively are derived as

$$ {}_ma_{23} = \begin{Bmatrix} C_{m\gamma_b} \cdot S_{m\phi_2} + S_{m\gamma_b} \cdot S_{m\phi_1} \cdot C_{m\phi_2} \\ S_{m\gamma_b} \cdot S_{m\phi_2} - C_{m\gamma_b} \cdot S_{m\phi_1} \cdot C_{m\phi_2} \\ C_{m\phi_1} \cdot C_{m\phi_2} \end{Bmatrix} \quad (4) $$

$$ {}_ma_{34} = \begin{Bmatrix} C_{m\gamma_b} \cdot S_{(m\phi_2 + m\phi_3)} + S_{m\gamma_b} \cdot S_{m\phi_1} \cdot C_{(m\phi_2 + m\phi_3)} \\ S_{m\gamma_b} \cdot S_{(m\phi_2 + m\phi_3)} - C_{m\gamma_b} \cdot S_{m\phi_1} \cdot C_{(m\phi_2 + m\phi_3)} \\ C_{m\phi_1} \cdot C_{(m\phi_2 + m\phi_3)} \end{Bmatrix} \quad (5) $$

where C and S denote cosine and sine, respectively.

After rearranging the Eq. (3), we get

$$ {}_mR_c - {}_mR_b = {}_mL_1 \cdot {}_ma_{23} + {}_mL_2 \cdot {}_ma_{34}. \quad (6) $$

Then, substitute ${}_ma_{23}$ and ${}_ma_{34}$ into Eq. (6). The components of the vector $({}_mR_c - {}_mR_b)$ are denoted as

$$ ({}_mR_c - {}_mR_b)_x = {}_mL_1(C_{m\gamma_b} \cdot S_{m\phi_2} + S_{m\gamma_b} \cdot S_{m\phi_1} \cdot C_{m\phi_2}) + {}_mL_2(C_{m\gamma_b} \cdot S_{(m\phi_2 + m\phi_3)} + S_{m\gamma_b} \cdot S_{m\phi_1} \cdot C_{(m\phi_2 + m\phi_3)}) \quad (7) $$

$$ ({}_mR_c - {}_mR_b)_x = {}_mL_1(S_{m\gamma_b} \cdot S_{m\phi_2} + C_{m\gamma_b} \cdot S_{m\phi_1} \cdot C_{m\phi_2}) + {}_mL_2(S_{m\gamma_b} \cdot S_{(m\phi_2 + m\phi_3)} - C_{m\gamma_b} \cdot S_{m\phi_1} \cdot C_{(m\phi_2 + m\phi_3)}) \quad (8) $$

$$ ({}_mR_c - {}_mR_b)_z = ({}_mL_1 \cdot C_{m\phi_2} + {}_mL_2 \cdot C_{(m\phi_2 + m\phi_3)}) C_{m\phi_1}. \quad (9) $$

From Eqs. (7) to (9), the ratio between $\sin({}_m\phi_1)$ and $\cos({}_m\phi_1)$ is obtained as

$$ \frac{\sin({}_m\phi_1)}{\cos({}_m\phi_1)} = \frac{({}_mR_c - {}_mR_b)_x \cdot S_{m\gamma_b} - ({}_mR_c - {}_mR_b)_y \cdot C_{m\gamma_b}}{({}_mR_c - {}_mR_b)_z}. \quad (10) $$

Therefore, the first joint angle is

$$ {}_m\phi_1 = a\tan2(\sin({}_m\phi_1), \cos({}_m\phi_1)). \quad (11) $$

Now, multiply Eqs. (7) and (8) by $\sin({}_m\phi_2)$ and $\cos({}_m\phi_2)$, respectively, and adding the result, we obtain

$$ A \cdot \sin({}_m\phi_2) + B \cdot \cos({}_m\phi_2) = C \quad (12) $$

where

$$ A = ({}_mR_c - {}_mR_b)_x \cdot C^m{}_{\gamma_b} + ({}_mR_c - {}_mR_b)_y \cdot S_{m\gamma_b} \quad (13) $$

$$ B = \frac{({}_mR_c - {}_mR_b)_z}{C_{m\phi_1}} \quad (14) $$

$$ C = \frac{A^2 + B^2 + {}_mL_1^2 - {}_mL_2^2}{2\,{}_mL_1}. \quad (15) $$

Let $t = \tan\frac{{}_m\phi_2}{2}$, then $\sin({}_m\phi_2) = \frac{2t}{1+t^2}$ and $\cos({}_m\phi_2) = \frac{1-t^2}{1+t^2}$. Substituting these expressions into Eq. (12) results in

$$t = \frac{A \pm \sqrt{A^2 + B^2 - C^2}}{B + C} \tag{16}$$

where '+' sign is chosen for the elbow-out configuration of Fig. 1, and the second joint angle is obtained as

$${}_m\phi_2 = 2\,\text{atan}(t). \tag{17}$$

Finally, the third joint angle is obtained by combining Eqs. (7) and (8), as

$${}_m\phi_3 = \text{atan2}({}_mL_2 \cdot S_{({}_m\phi_2 - {}_m\phi_3)}, {}_mL_2 \cdot C_{({}_m\phi_2 + {}_m\phi_3)}) - {}_m\phi_2 \tag{18}$$

where

$${}_mL_2 \cdot S_{({}_m\phi_2 - {}_m\phi_3)} = -{}_mL_1 \cdot C_{{}_m\phi_2} + \frac{({}_mR_c - {}_mR_b)_z}{C_{{}_m\phi_1}} \tag{19}$$

$$\begin{aligned} {}_mL_2 \cdot C_{({}_m\phi_2 + {}_m\phi_3)} = & -{}_mL_1 \cdot S_{{}_m\phi_2} \\ & + ({}_mR_c - {}_mR_b)_x \cdot C_{{}_m\gamma_b} \\ & + ({}_mR_c - {}_mR_b)_y \cdot S_{{}_m\gamma_b}. \end{aligned} \tag{20}$$

4.2 First-order kinematics

We define the output displacement vector as

$$u = (x_t, y_t, z_t, \theta_x, \theta_y, \theta_z)^T \tag{21}$$

where x_t, y_t and z_t represent the positions of the origin for the upper platform, and θ_x, θ_y and θ_z denote Euler angles equivalent to $[R_b^t]$. That is, $[R_b^t] = [Rot(x, \theta_x)][Rot(y, \theta_y)][Rot(z, \theta_z)]$.

The four contact points with the ball and socket joints are

$$c = ({}_1c^T, {}_2c^T, {}_3c^T, {}_4c^T)^T \tag{22}$$

where

$${}_mc = ({}_mx_c, {}_my_c, {}_mz_c)^T. \tag{23}$$

Each contact point vector is expressed as

$${}_mc = R_t + {}_mr_c, \quad {}_mr_c = [R_b^t]\,{}_mr_c^{(t)}. \tag{24}$$

Differentiating ${}_mc$ with respect to time results in

$${}_m\dot{c} = \dot{R}_t + \omega \times {}_mr_c \tag{25}$$

Where

$$\omega = (\omega_x, \omega_y, \omega_z)^T \tag{26}$$

and

$$\dot{R}_t = (\dot{x}_t, \dot{y}_t, \dot{z}_t)^T \tag{27}$$

$${}_mr_c = ({}_mr_{cx}, {}_mr_{cy}, {}_mr_{cz})^T. \tag{28}$$

Eq. (25) can be written in a matrix form as

$${}_m\dot{c} = [{}^mG_u^c]\,\dot{u} \tag{29}$$

where

$$[{}^mG_u^c] = \begin{bmatrix} 1 & 0 & 0 & 0 & {}_mr_{cz} & -{}_mr_{cy} \\ 0 & 1 & 0 & -{}_mr_{cz} & 0 & {}_mr_{cx} \\ 0 & 0 & 1 & {}_mr_{cy} & -{}_mr_{cx} & 0 \end{bmatrix}. \tag{30}$$

Then the relationship between $\dot{u}$ and $\dot{c}$ is denoted as

$$\dot{c} = [G_u^c]\,\dot{u} \tag{31}$$

where

$$[G_u^c] = [[{}^1G_u^c]^T [{}^2G_u^c]^T [{}^3G_u^c]^T [{}^4G_u^c]^T]^T. \tag{32}$$

Open-chain kinematics of each leg is described as

$${}_m\dot{c} = [{}_mG_\phi^c]\,{}_m\dot{\phi} \tag{33}$$

where the components of the $[{}_mG_\phi^c]$ matrix are developed in Appendix 1.

Assuming no singularity in $[{}_mG_\phi^c]$, a first-order inverse kinematic formulation is obtained as

$${}_m\dot{\phi} = [{}_mG_c^\phi]\,{}_m\dot{c}. \tag{34}$$

Now, the relationship between the active inputs and the c coordinates is denoted as

$$\dot{\phi}_a = [G_c^a]\,\dot{c} \tag{35}$$

where

$$\dot{\phi}_a = ({}_1\dot{\phi}_1, {}_1\dot{\phi}_2, {}_2\dot{\phi}_1, {}_2\dot{\phi}_2, {}_3\dot{\phi}_1, {}_3\dot{\phi}_2, {}_4\dot{\phi}_1, {}_4\dot{\phi}_2)^T \tag{36}$$

and

$$[G_c^a] = \begin{bmatrix} [{}^1G_c^\phi]_1: & 0 & 0 & 0 \\ [{}^1G_c^\phi]_2: & 0 & 0 & 0 \\ 0 & [{}^2G_c^\phi]_1: & 0 & 0 \\ 0 & [{}^2G_c^\phi]_2: & 0 & 0 \\ 0 & 0 & [{}^3G_c^\phi]_1: & 0 \\ 0 & 0 & [{}^3G_c^\phi]_2: & 0 \\ 0 & 0 & 0 & [{}^4G_c^\phi]_1: \\ 0 & 0 & 0 & [{}^4G_c^\phi]_2: \end{bmatrix}. \tag{37}$$

Substituting Eq. (31) into Eq. (35) yields the following relationship between the operational velocity ($\dot{u}$) and the active joint velocity ($\dot{\phi}_a$)

$$\dot{\phi}_a = [G_c^a]\,\dot{c} = [G_u^a]\,\dot{u} \tag{38}$$

where

$$[G_u^a] = [G_c^a][G_u^c]. \tag{39}$$

4.3 Scaling the components of the jacobian matrix

General spatial motion involves both translation and the rotation. Therefore, the Jacobian for this case has different units in the translational part and the rotational part. When the translational motion and the rotational motion are investigated separately, the result does not represent general 6-DOF motion characteristics. In order to treat the translational and the rotational part simultaneously, a Jacobian scaling technique based on the nominal value of the traslational (v_0) and the rotational velocity (ω_0) is employed here.

The scaled form of the oprational velocity vector is related to the original operational velocity vecotr as

$$\begin{pmatrix} v^* \\ \omega \end{pmatrix} = \begin{bmatrix} [\omega_0/v_0] & [0] \\ [0] & [I] \end{bmatrix} \begin{pmatrix} v \\ \omega \end{pmatrix} \tag{40}$$

where $[\omega_0/v_0]$ is a diagonal mitrix with each diagonal component's value being the same. Now, substituting Eq. (40) into Eq. (38) yields

$$\dot{\phi}_a = [G_u^a]\dot{u} = \begin{bmatrix} [G_v^a] \\ [G_\omega^a] \end{bmatrix} \begin{pmatrix} v \\ \omega \end{pmatrix} = [G_{u^*}^a] \begin{pmatrix} v^* \\ \omega \end{pmatrix} \tag{41}$$

where $[G_v^a]$ and $[G_\omega^a]$ correspond to the translational and rotational parts of $[G_u^a]$, respectively, and the scaled Jacobian is given as

$$[G_{u^*}^a] = \begin{bmatrix} [G_v^a] \\ [G_\omega^a] \end{bmatrix} \begin{bmatrix} [\omega_0/v_0] & [0] \\ [0] & [I] \end{bmatrix}^{-1} \tag{42}$$

By the same fashion, the scaled form of the operational load vector is related to the original operational load vector as

$$\begin{pmatrix} f^* \\ \tau \end{pmatrix} = \begin{bmatrix} [\tau_0/f_0] & [0] \\ [0] & [I] \end{bmatrix} \begin{pmatrix} f \\ \tau \end{pmatrix}. \tag{43}$$

The dual expression of Eq. (38) is given as

$$T_u = [G_u^a]^T T_a \tag{44}$$

where

$$T_u = \begin{pmatrix} f \\ \tau \end{pmatrix}. \tag{45}$$

Now, substituting Eqs. (43) into Eq. (44) yields

$$\begin{pmatrix} f^* \\ \tau \end{pmatrix} = [G_{u^*}^a]^T T_a \tag{46}$$

where the scaled Jacobian is given as

$$[G_{u^*}^a]^T = \begin{bmatrix} [\tau_0/f_0] & [0] \\ [0] & [I] \end{bmatrix} [G_u^a]^T \tag{47}$$

It is derived from Eqs. (42) and (47) that a dual relation exists between the translational and the rotational parts. Therefore, a scaling factor can be chosen according to the desired application. For example, based on rough dexterous motion of the human arm, the nominal translational and rotational velocities are estimated to be 40 in/sec and 6 rad/sec, respecitively (Parsons, 1985). This ratio can be employed as the scaling factor in the design of a force reflecting manual controller mechanism. When the ratio of the torque (τ_0/f_0) is based on the desired force-reflecting capability, the required actuator torques could be minimized. For example, the average values of force range of the human right arm in an aircraft control stick, 15.5" in fron of seated subject, are :

- 96.3, 83.3 lb for pushing, pulling,
- 38., 29. lb for force to left, right,
- 1.09 lb-ft for maximum torque on a 2" diameter knob(Parsons, 1985).

Several other candidates can possibly be employed as a scaling factor.

5. Geometric Criteria

One of the basic aspects of minipulator design is determining the workspace. Many researchers have defined the concept of workspace(Gupta and Roth, 1982; Kumar and Waldron, 1981; Parden and Sastry, 1989; Vijaykumar et al., 1986). The operating region or workspace of a manipulator is characterized by a reachable workspace and a dexterous workspace(Vijaykumar, 1986). The reachable workspace is defined as the volume or space within which a reference point on the hand (end-effector) can be made to coincide with any point in space. The dexterous workspace is the volume within which the robot hand has complete manipulative capability. With a reference point in the dexterous workspace, the hand can be completely rotated about any axis through that point. A manipulator should be designed so that it has the well-connected workspace property

which allows its end-effector to move from one regular value to another without passing through a critical value (singularity). Thus, Parden and Sastry(1989) defined the maximal work-volume index in the light of this aspect.

In this paper, a dexterous workspace is numerically calculated, and a feasible workspace is chosen based on composite design indices which qualitatively combine the dexterous workspace and other important design criteria, such as global isotropic index, maximum force trasmission ration, and so on.

Types of singularity have been defined in both serial and parallel manipulators. Several criteria have been developed to detect the singular configurations of the robot (Cox, 1981; Gupta and Roth, 1982; Kumar and Gardner, 1990; Mohammed, 1983). In robot design, much effort has been paid to eliminate singularities within the workspace. Specifically, Serial structures have been investigated concerning configuration-dependent singularity. Structurally, parallel mechanisms consists of several open-chain serial structures. This type of mechanism possesses additional forms of singularities due to the interaction among those open-chains, such as stationary and uncertainty cofiguration(Cox, 1981; Kumar and Gardner, 1990; Mohammed, 1983), algorithmic singularity (Meyer and Angeles, 1989), and architectural singularity (Ma and Angeles, 1991; Yi et al., 1992). Specifically, the architectural singularity has been conceived, by many designers, in the design of the Stewart platform manipulator (Fig. 3) in which each leg consists of a passive hooke joint in the base platform site, an active prismatic joint in the connecting link, and a passive ball and socket joint in the upper platform site.

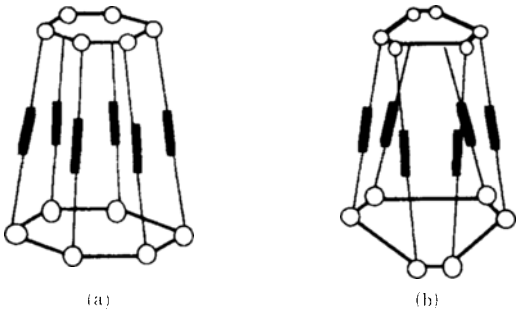

Fig. 3 Stewart platform manipulator

The configuration of Fig. 3(a) suffers from the so-called "architectural singularity". This kind of singularity occurs when the instantaneous screws of the activated prismatic joints meet at a point in the operational space, and therfore, the operational moment components cannot be properly controlled. This problem could be resolved by the architecture of Fig. 3(b), in which the directions of the instantaneous screws are spread out in the operational space, in order to avoid the situation of the former case. Ma and Angeles(1991) analytically demonstrated the beneficial aspects of the architecture of Fig. 3(b).

The configurations of Fig. 4(b) and Fig. 4(c) are the planar view of the manipulator of Fig. 4(a), illustrating the stationary and the uncertainty configurations of this manipulator, respectively. The architectural singularity of the proposed manipulator can be avoided by properly locating the actuator site, while in the Stewart platform design the architectural singularity can be minimized by changing the structures of the manipulator. In section 8, optimal design parameters of this manipulator will be obtained such that the manipulator possesses a maximum workspace

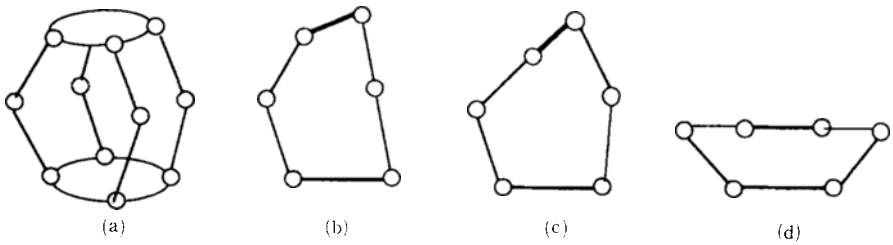

Fig. 4 Configuration-dependent singularity

with least potential for singularity.

6. Kinematic Criteria

Based on the effective force relationship (Eq. (44)) between the operational force vector and the input force vector, the ratio of the 2-norm of the output load (T_u) to that of the input load (T_a) can be expressed as

$$\frac{\|T_u\|}{\|T_a\|}=\left\{\frac{T_a^T[G_u^a][G_u^a]^T T_a}{T_a^T T_a}\right\}^{1/2}. \tag{48}$$

Based on the Rayleigh quotient(Strang, 1980), the output bounds with respect to the input loads are given as

$$\sigma_{\min}\|T_a\|\leq\|T_u\|\leq\sigma_{\max}\|T_a\| \tag{49}$$

where $\sigma_{\min}$ and $\sigma_{\max}$ are the square roots of the minimum and maximum singular values of $[G_u^a][G_u^a]^T$, respectively. Since $[G_u^a][G_u^a]^T$ is an 8 $\times$8 matrix and has rank six, two singular value are always zero. The nonzero singular values of the 6 $\times$6 matrix $[G_u^a]^T[G_u^a]$ are the same as those of $[G_u^a][G_u^a]^T$. Thus, the nonzero singular values are obtained in terms of $[G_u^a]^T[G_u^a]$, and these singular values are used in determining the bounds of the force transmission ratio. An alternative expression of Eq. (49) is

$$\sigma'_{\min}\|T_u\|=\frac{\|T_u\|}{\sigma_{\max}}\leq\|T_a\|\leq\frac{\|T_u\|}{\sigma_{\min}}=\sigma'_{\max}\|T_u\| \tag{50}$$

where $\sigma'_{\max}(=\frac{1}{\sigma_{\min}})$ and $\sigma'_{\min}(=\frac{1}{\sigma_{\max}})$ denote the maximum and minimum force trasmission ratios (actuator capacities for an unit operational load of $\|T_u\|$), respectively.

6.1 Single design indices

6.1.1 Global condition number

The condition number is defined as the ratio of the maximum singular value to the minimum singlar value of the system Jacobian, given by

$$C=\frac{\sigma_{\max}}{\sigma_{\min}},\quad C\geq 1. \tag{51}$$

The global condition number (GC) is defined with respect to the entire workspace of the manipulator as

$$GC=\frac{\int_w C dW}{\int_w dW} \tag{52}$$

where $\int_w dW$ is the volume of the workspace of the manipulator.

6.1.2 Global isotropic index

The isotropic index is an important criterion of the performance for a manipulator. The isotropic index is defined as the inverse of the condition number and provides a measure of the shape of the transmission ellipsoid

$$S=\frac{\sigma_{\min}}{\sigma_{\max}},\quad 0\leq S\leq 1. \tag{53}$$

The global isotropic index (GI) is defined with respect to the entire workspace of the manipulator as

$$GI=\frac{\int_w S dW}{\int_w dW}. \tag{54}$$

6.1.3 Global maximum force transmission ratio

The actuator capacity of the manipulator is another important design criterion. The maximum force transmission ratio is defined, in Eq. (50), as the requred actuator capacity for an unit operational load of $\|T_u\|$. The global maximum force transmission ratio (GMFT) is defined with respect to the entire workspace of the manipulator as

$$GMFT=\frac{\int_w \sigma'_{\max} dW}{\int_w dW}. \tag{55}$$

The design of a mainpulator system can be based on any particular criterion. However, the single criterion based design does not provide sufficient control on the range of the design parameters involved. Therefore, multi-criteria based design has been proposed(Kurz and Hayward, 1992). However, the previous multi-criteria methods did not provide any systematic design procedure and flexibility in design. In the light of these facts, a concept of composite design index is proposed in the following section.

6.2 Composite design index

After the above global indices are evaluated, several composite indices can be developed by combining some of the above indices. However, various design indices are usually incommensurate concepts due to differences in unit and physical meanings, and therefore should not be combined with normalization and weighting func-

tions unless they are transferred into a common domain. In other words, quantitative combination should be avoided. Instead, these design indices should be combined qualitatively. As the inital step to this process, preferential information should be given to each design parameter and design index(Terano, et al. 1992; Wood, 1989). Then, each design index is transferred to a common preference design domain which ranges from zero to one. Here, the preference given to each design criterion is very subjective to the designer. Preference can be given to each criterion by weighting. This provides flexibility in design. The composite design index is developed in the following.

The general design index (CDI) is formed by combining all of the design indices. For example, a general design index which takes into account the workspace, the global isotropic index, and the global maximum force transmission ratio can be constructed as follows

$$CDI = \tilde{W} \wedge \tilde{GI} \wedge \tilde{GMFT} \tag{56}$$

where $\wedge$ denotes the "intersection" operation(Terano, et.al. 1982), and $\tilde{W}$, $\tilde{GI}$ and $\tilde{GMFT}$, given by

$$\tilde{W} = \frac{W - W_{\min}}{W_{\max} - W_{\min}} \tag{57}$$

$$\tilde{GI} = \frac{GI - GI_{\min}}{GI_{\max} - GI_{\min}} \tag{58}$$

$$\tilde{GMFT} = \frac{GMFT_{\max} - GMFT}{GMFT_{\max} - GMFT_{\min}} \tag{59}$$

denote a volume of the workspace, a global workspace, and a global maximum force transformation ratio, respectively, which are transfered to the same preference domain.

Note that each composite design index is constructed such that a large value represents a better design. Large $\tilde{W}$ implies that the system possesses a large workspace, large $\tilde{GI}$ implies that the system possesses good isotopic characteristic within the given workspace, and large $\tilde{GMFT}$ implies that the system requires small actuator effort to support an unit operational load within the given workspace. Therefore, large CDI implies that the system simultaneously possesses a large workspace, a good isotopic characteristic, and requires small actuator effort to support an unit operational load, within the given workspace.

A weighted composite design index($WCDI$) can also be considered. For instance, any of the single kinematic indices, which is included in the construction of the design index, can be given more weighting compared to the others. This weighting represents the significance of the index. A weighted composite design index can be represented as follows

$$WCDI = \tilde{W}^{\alpha} \wedge \tilde{GI}^{\beta} \wedge \tilde{GMFT}^{\gamma} \tag{60}$$

where α, β and γ represent the degrees of the weighting, and usually large values imply large weighting.

7. Dimensional Synthesis

Previous design experiences by many researchers (Kim, 1989; Ma and Angles, 1991; Parden and Sastry, 1989; Yi et al., 1992) illustrated that manipulator architecture should be the first step in design, and that dimensional and structural synthesis should come next. Therefore, manipulator types will be studied first with respect to the workspace, singularity, and force and velocity transmission capability. Based on the initial analysis, a set of optimal kinematic parameters is obtained by employing a composite design index. An alternative design with different design parameters is also investigated. Two designs are compared in terms of the local characteristics, such as local workspace, local dexterity, and local force transmission ratio.

7.1 Initial analysis-manipulator architecture

Table 1 illustrates several manipulator types with different kinematic dmensions. In the following analysis, we assume that the area below the lower platform is considered to be the ground (an obstacle) and the heights of each manipulator type are the same.

Figures (a) and (b) of Table 1 illustrate the first type. They have equal upper and lower platform radii with different link ratios. The configuration of Fig. (b) has larger workspace than that of Fig. (a). However, the configuration of Fig. (b) has a

Table 1 Manipulator type analysis

Configuration	Dimensions	Isotropy	Force Trans. Capability	Workspace
(a)	$L1 < L2$ $rt = rb$	Better	Better	
(b)	$L1 > L2$ $rt = rb$			Larger
(c)	$L1 = L2$ $rt < rb$			Larger
(d)	$L1 = L2$ $rt > rb$	Better	Better	
(e)	$L1 = L2$ $rt = rb$: Small	Worse		Larger
(f)	$L1 = L2$ $rt = rb$: Medium			
(g)	$L1 = L2$ $rt = rb$: Large	Worse	Better	
(h)	$L1 \ll L2$ $rt \ll rb$	Bad	Bad	
(i)	$L1 \gg L2$ $rt \ll rb$	Bad	Bad	Larger

singular region in the middle of its workspace when the upper two links become parallel to the upper platform. Therefore, the global isotropy of Fig. (b) is worse than that of Fig. (a). When the lower link of Fig. (b) rotates a little, the upper link rotates a lot. This implies that the configuration of Fig. (b) has better velocity transmission characteristic than that of Fig. (a). On the other hand, the configuration of Fig. (a) has better force transmission due to the dual relationship between force and velocity transmission. In other words, it requires a smaller actuation effort to support a given operation load.

As the second type, the cases with equal link lengths and different radii are analyzed. The configuration of Fig. (c) has larger workspace than that of Fig. (d). When the lower link of Fig. (c) rotates a little, the upper link rotates a lot. Therefore, the configuration of Fig. (c) has better velocity transmission characteristic than that of Fig. (d). On the contrary, the configuration of Fig. (d) has better force transmission due to the dual relationship between the force and velocity transmission.

As observed from the above analysis, each case of the two types has good and bad aspects. None of the above types simultaneously satisfy a large workspace, good isotropy, and a small force transmission ratio.

In this work, we pursue a design which evenly satisfies the above three criteria. The cases of Figs. (e), (f) and (g) illustrate the configurations which have equal link lengths and equal radii, respectively. This type is shown to be the compromise between the previous types. The configuration of Fig. (e) has the largest workspace among three cases, while that of Fig. (g) has a good force transmission capability since it requires the smallest force transmission ratio due to the large force leverage in the upper platform. The types of Figs. (e) and (g) are not desirable with respect to isotropy, since both cases are easily confronted with singular configurations as shown in Fig. 4. From the above analysis, an in-between configuration like that of Fig. (f) is shown to be the best compromise.

The configurations of Figs. (h) and (i) illustrate extreme cases, which have different radii and different link lengths with large dimensional ratios. In general, these types are not recommended since the overall characteristics are not satisfactory. However, considering a specific application (e.g., big velocity transmission capability or large workspace) with sacrifice of the other desirable properties, one of these cases can possibly be chosen.

7.2 Initial design

In this section, the design will be performed with the third type of Table 1 which has the same radii and the same link lengths. An optimal ratio between the link length and the radius will be decided in order to satisfy the above three criteria evenly. As an application example, we are interested in the design of a force reflecting manual controller mechanism. Therefore, the scaling factor given by the manipulator specifications will be employed.

The range of the two parameters (i.e., radius and link length) is from 5 inches to 14 inches. Figures 5(a), (b) and (c) illustrate the plots for the dexterous workspace, the global isotropic index, and the global maximum force transmission ratio of the example mechanism, respectively, which are transferred to the preference domain ranging from zero to one. Here, the best preference is given to the maximum value of dexterous workspace and global isotropic index, and the least preference is given to the minimum value of

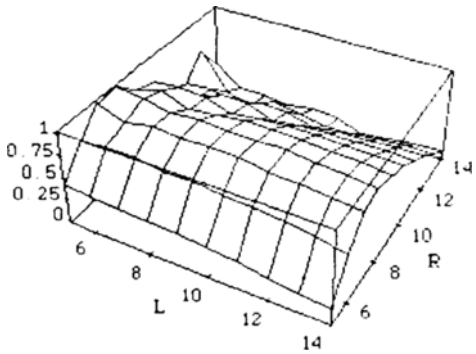

(a) Grobal isotropic index

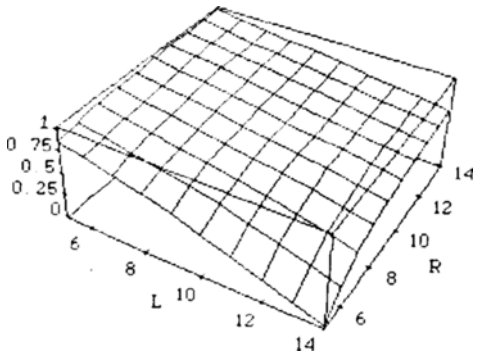

(b) Grobal maximum force transmission ratio

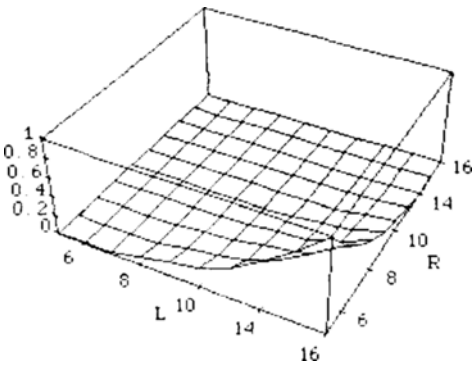

(c) Dexterous workspace

Fig. 5 Global design indices for initial design in preference domain

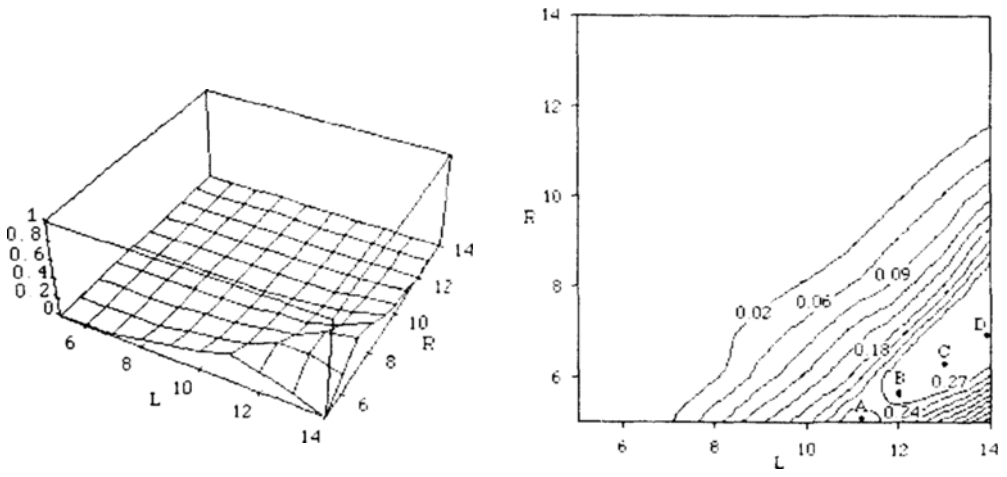

Fig. 6 Composite disign index for initial design

those design criteria. On the other hand, the best preference is given to the minimum value of the global maximum force transmission ratio, and the least preference is given to the maximum value of that design criterion, because small force transmission (small actuator size, herein) is preferred. As mentioned in Section 6, the designer has some flexibility in deciding the preference level for each design criteria.

In the simulation, the entire six dimensions of the operational space are searched to obtain the global indices. Eleven points are evaluated in each direction. The trends are coincident with that of the initial analysis which was based on simple geometric inspection. Specifically, it turns out that an optimal region exists with respect to the global isotropic index.

Now, the composite design indices developed in Section 6 can be employed to obtain a set of optimal design parameters. Figure 6 illustrates the composite design index plot which combines the three design criteria (i.e., isotropy, force transmission, and dexterous workspace) with the same weighting. An optimal region exists along the top of the hill. Four design candidates are chosen in Table 2. Here, the dimension of the radius affects the actuator size, because the size of the lower platform is determined by the size of the gimbal mechanism. Therefore, the size of the radius should be big enough to satisfy the platform size constraint. Case C is chosen as an illustrative example in the following analysis.

An algorithm to obtain a set of optimal design parameters is summerized as follows :

(1) Considering the maximum height (30") of the system, a volume with $30" \times 60" \times 60"$ is chosen as a candidate for the system workspace. Each operational space is divided into eleven points.

(2) For a given operational positions (three translational positions and three rotational positions), calculate the joint angles for each leg. If all of the joint angles exist, then calculate Jacobian and inverse Jacobian of each leg and increment the number of the available workspace with an unit volume, else go to next operational position and repeat step(2).

(3) Construct the system Jacobian of Eq. (37). Using SVD scheme, obtain the singular values of the system Jacobian, and then calculate the values of the single design indices.

(4) Calculate the values of the global design indices, calculate the value of composite design index, and then employ a nonlinear programming technique to find a set of optimal design parameters.

Table 2 Design candidates for initial design

	A	B	C	D
L	11"	12"	13"	14"
R	5"	6"	6.5"	7"

(For the current case with only two design parameters, a set of optimal parameters can be obtained by inspection of the three dimensional plot of Fig. 6, which represents the composite design index plot combining the three design criteria.)

7.3 Second design

The initial analysis illustrated that the manipulator with different link lengths or different radii represented a conflict among the three basic design criteria. In this section, our design will be

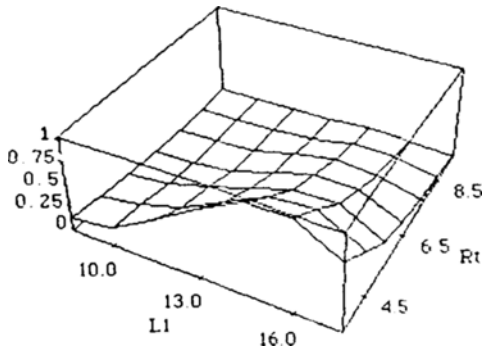

(a) Grobal isotropic index

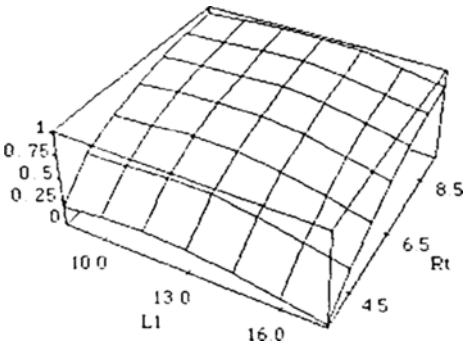

(b) Grobal maximum force transmission ratio

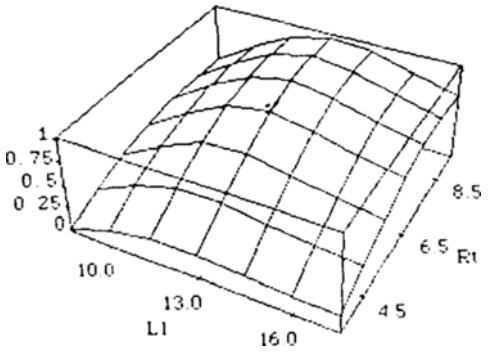

(c) Dexterous workspace

Fig. 7 Global design indices for secondary design in preference domain

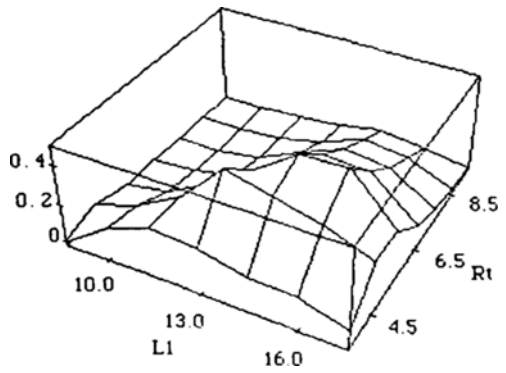

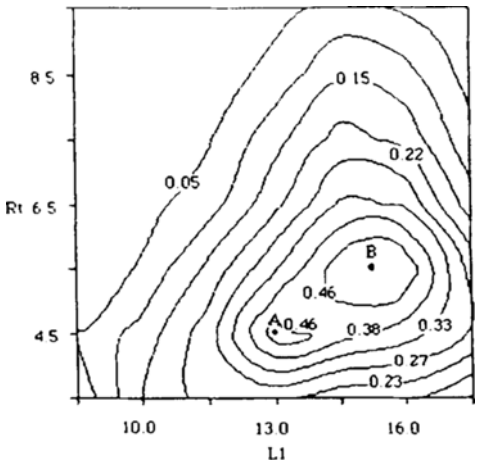

Fig. 8 Composite design index for secondary design

based on the first and the second types of Table 1, and this design will be compared to the initial design.

Four design parameters (i.e., L_1, L_2, R_t, R_b) are employed, and two constraints are included to reduce the number of design parameters. These two constraints are based on the initial design. The height of the manipulator is set to be a constant value 26 inches, and the lower radius is set to be 6.5 inches. Therefore, there exists only two independent design parameters (e.g., either L_1 and R_t or L_2 and R_t).

Figure 7 illustrates the three global design indices which are transferred to the preference domain. Again, a composite design index plot which is also based on the three design criteria is employed to obtain an optimal set of design parameters.

Figure 8 displays the composite design index plot in which the areas surrounding the two peaks denote the optimal regions. Two candidate points are suggested in Table 3. Case B has better isotropy and force transmission capability but has a less dexterous workspace, compared to that of case A. However, since the second link for case B is shorter than that of case A, a less isotropic dexterous workspace exists in the upper part of the workspace. Instead, that workspace is spread out in other parts of the workspace. Therefore, if a larger dexterous workspace is required in the upper workspace, the design of case A is appropriate. Our design can also be based on a local workspace insead of the whole workspace. If the design is based on only the upper part of the whole workspace, the solution should be coincident to case A.

Table 3 Design candidates for secondary design

	A	B
L1	13"	14.5"
Rt	4.5"	5.5"

7.4 Comparison of the two designs

In the previous section, the designs have been pursued by evaluating the global properties. However, the global properties do not represent the local characteristics of the manipulator. In this section, the local characteristics of the first and the second designs will be analyzed in part by examining the global X-Z plane of the given manipulator in Fig. 1.

First, the local characteristics of the manipulator will be examined in terms of the global X and Z coordinates, and the rotation angle θ_y about the global Y axis. Figures 9(a) and (b) illustrate the isotropic index and the maximum force transmission ratio plots in the X-Z plane for the initial design ($L_1=13$" and $R_t=6.5$"), respectively. These plots are obtained as follows : for each point of the X-Z plane the rotation angle θ_y about the global Y axis is incremented from $-45°$ to $45°$, and the singular values are calculated for each θ_y. The maximum and minimum singular

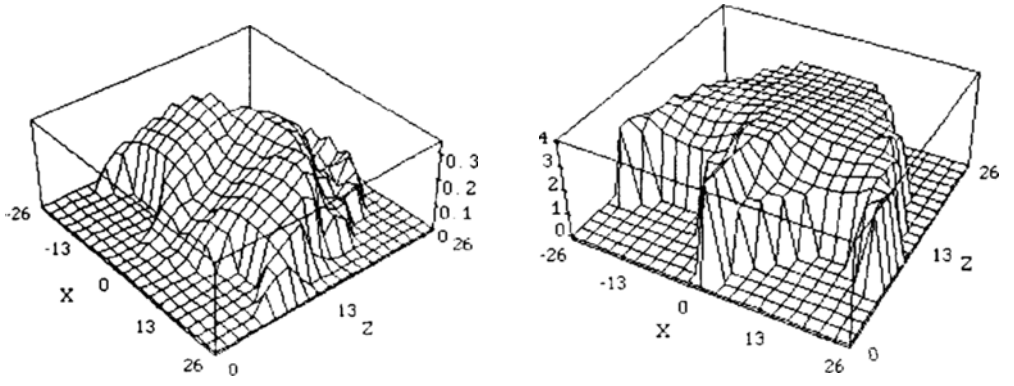

(a) Local isotropic index plot (b) Local maximum force transmission ratio plot

Fig. 9 Analysis of X-Z plane for the initial design

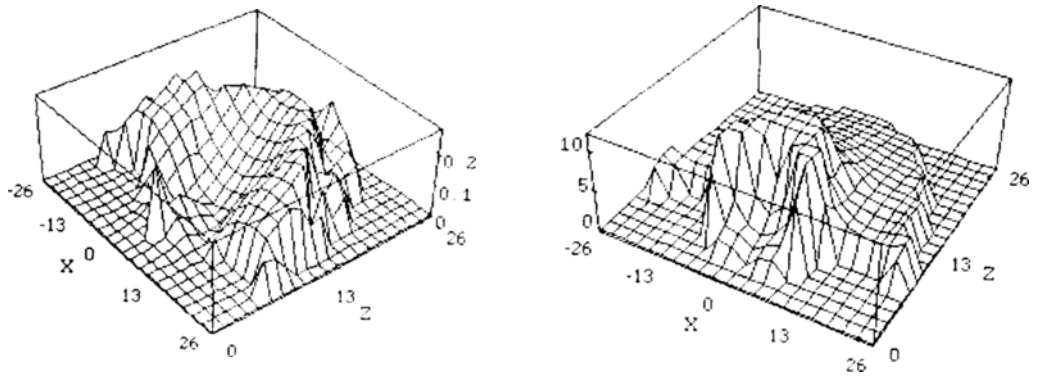

(a) Local isotropic index plot (b) Local maximum force transmission ratio plot

Fig. 10 Analysis of X-Z plane for the secondary design

values are selected from this set, and the isotropic index is obtained from these values. Thus, these values are used as the contour height for the given value of the X-Z plane. It is shown from the isotropic index plot of Fig. 9(a) that good isotropic region is located in the upper part of the workspace. On the other hand, the global maximum force transmission characteristic, as shown in Fig. 9(b), is shown to have even distribution throughout the entire workspace. The upper flat regions of these plots represent the space that has greater force transmission ratios than the acceptable threshold value (e.g., 10). The lower flat resions of these plots denote the out-of-bound workspace that the mechanism cannot reach.

Figures 10(a) and (b) illustrate the isotropic index and the maximum force transmission ratio plot in the X-Z plane for the secondary design ($L_1=14.5$" and $R_t=5.5$"), respectively. It is shown that the secondary design has poorer isotropy and force transmission characteristics, while the dexterous workspace is about two times larger than that of the initial design. Therefore, if more weighting is given to the isotropic and force transmission characteristics, the design will approach the case of the initial design.

8. Fault Tolerance Based Analysis

The proposed mainipulator system has fault-tolerant capability due to the two redundant actuators. In this section, the fault-tolerant capability of this manipulator will be analyzed. The optimal kinematic dimensions obtained in the

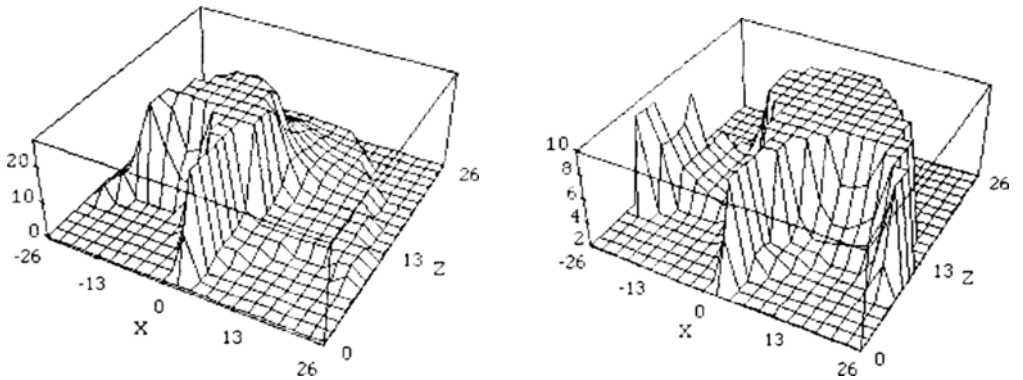

(a) Failure at ${}_1\phi_1$ (b) Failure at ${}_1\phi_2$

Fig. 11 Fault-tolerant analysis

initial design procedure will be employed.

Fault-tolerant capability will be measured in terms of the maximum force transmission ratio (MFTR) in the global X-Z plane. Initially, one complete failure of the system actuator will be considered. Figure 11 illustrates the MFTR of four possible (one complete) failure cases. The failures of the first and second joint actuators of the first chain greatly deteriorate the MFTR of the manipulator.

In order to improve the fault-tolerant capability of the system, the concept of prime mover duality is introduced as the lowest level of redundancy for Fault tolerance(Sreevijayan, 1992). We employ a double-sided symmetric actuator system with independent electronic controllers for each side. This module, being developed at the University of Texas at Austin, has the attributes of compactness, high stiffness, low weight and minimum interface to the system controller. If one half of the module fails, the other half picks up the load in parallel. This duality at the actuator level allows a complete failure of one side of the dual system to be overcome by doubling up on the other side in a short period of time or by providing more actuation effort from the other base actuators.

Figure 12 illustrates the possible cases of distributed failures. Here, the force transmission capabilities for these cases will be compared to those of the one complete failure cases. First of all, the bounds of the force transmission ratios for these cases need to be reformulated by considering the information of the distributed failure. An alternative form of Eq. (54) is as follows

$$T_v=[G_u^a]^T T_a=[G_u^a]^T[S]\,T_a^F \tag{61}$$

where

$$[S]=\begin{bmatrix} a_1 & 0 & \cdots & 0 \\ 0 & a_2 & & \\ \vdots & & \ddots & \\ 0 & & & a_8 \end{bmatrix} \tag{62}$$

and

$$T_a^f=(\frac{{}_1T_1}{a_1},\ \frac{{}_2T_1}{a_2},\ \cdots,\ \frac{{}_8T_1}{a_8})^T \tag{63}$$

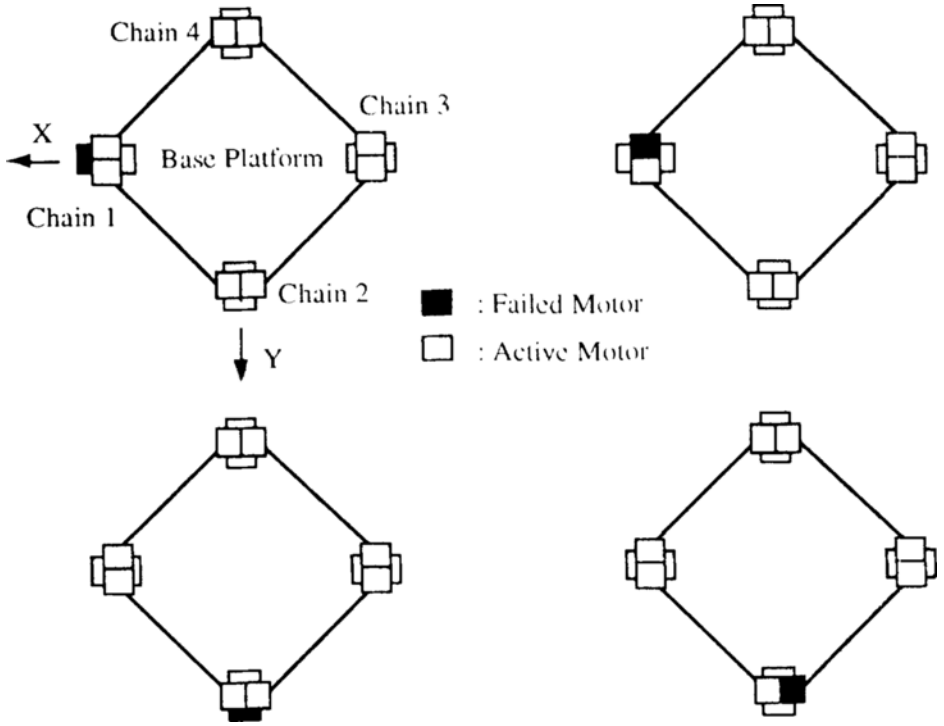

Fig. 12 Distriguted failure cases

with $a_1, a_2, \cdots, a_8$ being nonzero scalar quantities, less than or equal to one. These values can be used to carry the information of actuator or relative actuator sizes. A solution for T_a^F is obtained by minimizing a quadratic scalar quanitity $(T_a^F)^T T_a^F$, subject to the constraint Eq. (61).

Assuming only one half failure at the base axis of the fourth chain, the values of $a_1, a_2, \cdots, a_7$ in the $[S]$ matrix are 1, and that of a_8 is 0.5. Physically, this weighting matrix penalizes the actuation effort of the last axis twice as much as that of the other axes, which restricts the torque capacity of the actuator on the last axis to 50% of the other actuators.

A new force transmission relationship between T_u and T_a should be formulated, which includes the information of any possibility of partial joint failure. First of all, the force transmission ratio between T_u and T_a^F is determined, and is expressed as

$$\frac{\|T_u\|}{\|T_a^F\|} = \left(\frac{(T_a^F)^T [S]^T [G_u^a][G_u^a]^T [S] T_a^F}{(T_a^F)^T T_a^F} \right)^{1/2} \tag{64}$$

Also, based on the Rayleigh quotient, the output bounds with respect to the input loads are given as

$$s_{\min}^F \|T_a^F\| \leqq \|T_u\| \leqq s_{\max}^F \|T_a^F\| \tag{65}$$

where $s_{\min}^F$ and $s_{\max}^F$ are the square roots of the minimum and maximum singular values, respectively, of $[S]^T[G_u^a][G_u^a]^T[S]$. Only nonzero singular values are treated in determining the force transmission ratio. An alternative expression of Eq. (65) is

$$\frac{\|T_u\|}{s_{\max}^F} \leqq \|T_a^F\| \leqq \frac{\|T_u\|}{s_{\min}^F}. \tag{66}$$

As the second step, the force transmission relationship between T_a and T_a^F is considered, and it is given by

$$\frac{\|T_a\|}{\|T_a^F\|} = \left(\frac{(T_a^F)^T [S]^T [S] T_a^F}{(T_a^F)^T T_a^F} \right)^{1/2} \tag{67}$$

where the bounds of T_a with respect to T_a^F are given as

$$s_{\min}^W \|T_a^F\| \leqq \|T_a\| \leqq s_{\max}^W \|T_a^F\|. \tag{68}$$

Here, $s_{\min}^W$ and $s_{\max}^W$ are the square roots of the minimum and maximum singular values of $[S]^T[S]$, respectively. For one half failure at the base axis of the fourth chain, the values of $s_{\min}^W$ and $s_{\max}^W$ are 0.5 and 1.0, respectively. $s_{\min}^W$ is always less than or equal to 1 for any failure case, thus, $\|T_a^F\|$ is always equal to or greater than $\|T_a\|$.

Combining the results of Eqs. (66) and (68) yields the bounds of $\|T_a\|$ with respect to $\|T_u\|$ as follows

$$\frac{s_{\min}^W}{s_{\max}^F} \|T_u\| \leqq \|T_a\| \leqq \frac{s_{\max}^W}{s_{\min}^F} \|T_u\| \tag{69}$$

where $s_{\max}^W$ is equal to one for the cases with one, two, or three half failures.

For simplicity, a single half failure case is considered. Figure 13 shows the maximum force transmission ratio plots for the cases with one

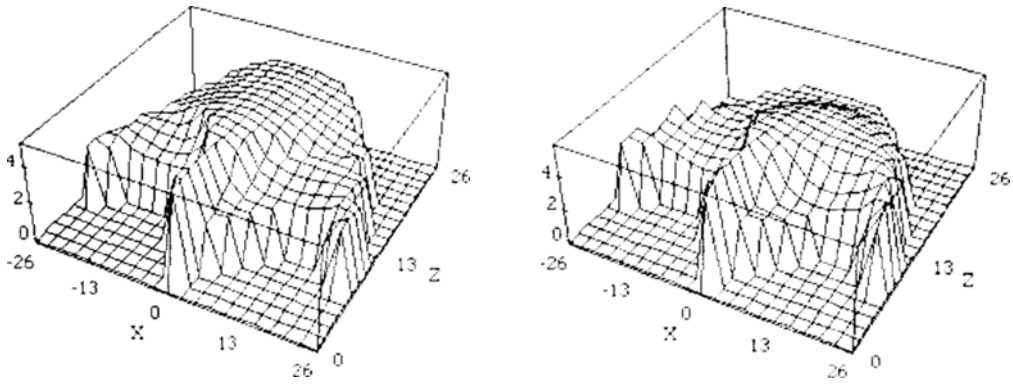

(a) Malf failure at ${}_1\phi_2$ (b) Malf failure at ${}_1\phi_2$

Fig. 13 Half failure cases

half failure. A slightly increased, but still good, force transmission capability (i.e., the magnitude of the required actuator size is smaller than that of one complete failure case) is illustrated. Further study illustrates that the force transmission ratio is gradually increased as the number of half failures increases; however, the force transmission capability of the case is still superior to that of the case with a complete failure.

9. Summary and Conclusion

Dimensional synthesis of a four-legged six degree of freedom parallel manipulator is investigated in this work. Initially, several types of manipulator architecture were reviewed. A concept of composite design index was incorporated into multi-criteria based design. This concept is shown to be a systematic tool for mechanism design, and possibly can be employed in other design optimization problems which consist of several design criteria.

Fault-tolerant capability due to force redundancy was also analyzed. Pime mover duality was introduced to dramatically increase the fault tolerance capability of this manipulator.

Acknowledgements

This paper was supported by NON DIRECTED RESEARCH FUND, Korea Research Foundation, 1993.

Appendix 1: Components of $[{}^{m}G_{\phi}^{c}]$

$$
\begin{aligned}
[{}^{m}G_{\phi}^{c}]_{1,1} &= ({}_{m}L_1 \cdot C_{m\phi_2} + {}_{m}L_2 \cdot C_{(m\phi_2 - m\phi_3)})\, S_{m\gamma_b} \cdot C_{m\phi_1} \\
[{}^{m}G_{\phi}^{c}]_{1,2} &= {}_{m}L_1 (C_{m\gamma_b} \cdot C_{m\phi_2} - S_{m\gamma_b} \cdot S_{m\phi_1} \cdot S_{m\phi_2}) + {}_{m}L_2 (C_{m\gamma_b} \cdot C_{(m\phi_2 + m\phi_3)} - S_{m\gamma_b} \cdot S_{m\phi_1} \cdot S_{(m\phi_2 + m\phi_3)}) \\
[{}^{m}G_{\phi}^{c}]_{1,3} &= {}_{m}L_2 (C_{m\gamma_b} \cdot C_{(m\phi_2 + m\phi_3)} - S_{m\gamma_b} \cdot S_{m\phi_1} \cdot S_{(m\phi_2 + m\phi_3)}) \\
[{}^{m}G_{\phi}^{c}]_{2,1} &= -({}_{m}L_1 \cdot C_{m\phi_2} + {}_{m}L_2 \cdot C_{(m\phi_2 + m\phi_3)})\, C_{m\gamma_b} \cdot C_{m\phi_1} \\
[{}^{m}G_{\phi}^{c}]_{2,2} &= {}_{m}L_1 (S_{m\gamma_b} \cdot C_{m\phi_2} + C_{m\gamma_b} \cdot S_{m\phi_1} \cdot S_{m\phi_2}) + {}_{m}L_2 (S_{m\gamma_b} \cdot C_{(m\phi_2 + m\phi_3)} + C_{m\gamma_b} \cdot S_{m\phi_1} \cdot S_{(m\phi_2 - m\phi_3)}) \\
[{}^{m}G_{\phi}^{c}]_{2,3} &= {}_{m}L_2 (S_{m\gamma_b} \cdot C_{(m\phi_2 + m\phi_3)} + C_{m\gamma_b} \cdot S_{m\phi_1} \cdot S_{(m\phi_2 - m\phi_3)}) \\
[{}^{m}G_{\phi}^{c}]_{3,1} &= -{}_{m}L_1 \cdot S_{m\phi_1} \cdot C_{m\phi_2} - {}_{m}L_2 \cdot S_{m\phi_1} \cdot C_{(m\phi_2 + m\phi_3)} \\
[{}^{m}G_{\phi}^{c}]_{3,2} &= -{}_{m}L_1 \cdot C_{m\phi_1} \cdot S_{m\phi_2} - {}_{m}L_2 \cdot C_{m\phi_1} \cdot S_{(m\phi_2 + m\phi_3)} \\
[{}^{m}G_{\phi}^{c}]_{3,3} &= -{}_{m}L_2 \cdot C_{(m\phi_1} \cdot S_{(m\phi_2 + m\phi_3)}).
\end{aligned}
$$

Appendix 2: Intersection Operator in Fuzzy Set Theory (Terano et al., 1992)

The intersection operator of two fuzzy sets A and B is defined by the following membership function:

$$\mu_{A \cap B}(x) = \mu_A(x) \wedge \mu_B(x) \tag{A1}$$

where the result of the intersection is the minimum value of the two membership functions (μ_A, μ_B), along the design parameter (denoted as "o" in Fig. 14). In Fig. 14, the intersection point "x" is shown to be the optimal design parameter which simultaneously satisfies the two design criteria A and B. The principle of Eq. (A1) applies to the case with more than two design criteria.

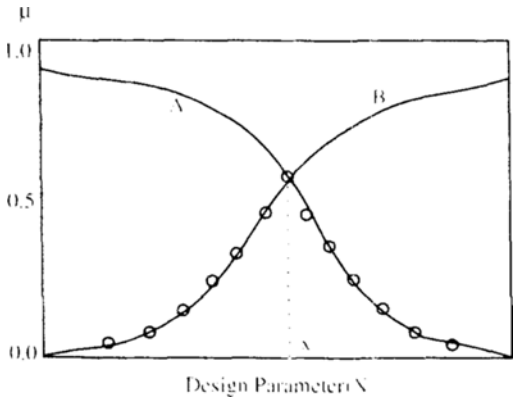

Fig. 14 Intersection of two fuzzy set

References

Cox, D., 1981, "The Dynamic Modeling and Command Signal Formulation for Parallel Multi-Parameter Robotic Devices," Master Thesis, Department of Mechanical Engineering, Univ. of Florida, Gainsville, FL.

Freeman, R. A. and Tesar, D., 1988, "Dynamic Modelling of Serial and Parallel Mechanisms/ Robotic Systems, Part I-Methodology, Part II-Application," *Trends and Developments in Mechanisms, Machines, and Robotics, 20th. Biennial Mechanisms Conf., Kissimmee*, FL. DE. Vol. 15~2, pp. 7~21.

Gosselin, C. and Angeles, J., 1987, "The Optimal Kinematic Design of a Spherical Three-Degree-of Freedom Parallel Manipulator," *ASME Advances In Design Automation : Robotics, Mechanisms, and Machine System*, DE-Vol. 10~2, pp. 111~115.

Gupta, K. C. and Roth, B., 1982, "Design Considerations for Manipulator Workspace," *ASME Journal of Mechanical Design*, Vol. 104, pp. 704~711.

Han, C. S., Tesar, D. and Traver, A. E., 1989, "The Optimal Design of a 6 DOF Fully Parallel Micro Manipulator for Enhanced Robot Accuracy," *ASME 1989 Design Automation Conference*, Montreal, CANADA, pp. 17~20.

Hunt, K. H., 1983, "Structural Kinematics of in-Parallel-Actuated Robot Arms," *Trans. ASME J. Mech., Transmission, Automation in Design*, VOl. 105, pp. 705~712.

Kim, W. K., 1989, "Architectural Study of the Design and Operation of Advanced Force Feedback Manual Controllers," Ph. D Dissertation of Mechanical Engineering, The Univ. of Texas at Austin.

Klein, C. A. and Blaho, B. E., 1987, "Dexterity for Design and Control of Kinematically Redundant Manipulator," *Int. Journal of Robotics Research*, Vol. 6, No. 2, pp. 72~83.

Kumar, A. and Waldron, K. J., 1981, "The Workspace of a Mechanical Manipulator," *ASME J. Mechanical Design*, Vol. 103, pp. 665~672.

Kumar, V. J. and Gardner, J., 1990, "Kinematics of Redundantly Actuated Closed Chains," *IEEE J. of Robotics and Automation*, Vol. 6, No. 2, pp. 269~273.

Kurz, R. and Hayward, W., 1992, "Multiple-Goal Kinematic Mechanism Optimization of a Parallel Spherical Mechanism with Actuator Redundancy," *Trans. on IEEE Journal of Robotics and Automation*, Vol. 8, No. 5, pp. 644~651.

Ma, O. and Angeles, J., 1991, "Architectural Singularities of Platform Manipulators," *Proc. IEEE Int. Conf. on Robotics and Automation*, Sacramento, CA, Vol. 2, pp. 1542~1547.

Meyer, A. N. and Angeles, J., 1989, "Force Optimization in Redundantly-Actuated Closed Kinematic Chains," *Proc. IEEE Conf. on Robotics and Automation*, Scottsdale, AZ, Vol. 1, pp. 951~956.

Mohammed, M. G., 1983, "Instantaneous Kinematics and Joint Displacement Analysis of Fully-Parallel Robotic Devices," Ph. D. Dissertation, Department of Mechanical Engineering, Unversity of Florida, Gainsville.

Parden, B. E. and Sastry, S., 1989, "Optimal Kinematic Design of 6R Manipulators," *Int. Journal of Robotics Research*, 7(2) : 43~61.

Parsons, H. M., 1985, "Human Factors Engineerng Issues in Army Field Robotics Applications," Prepared for the U.S. Army Human Engineering Laboratory, Aberdeen Proving Ground, MD. Huntsville, AL. Essex Corp.

Sreevijayan, D., 1992, "On the Design of Fault-Tolerant Robotic Manipulator Systems," M. S. Thesis, Dept. of Mechanical Eng., University of Texas at Austin.

Stewart, D., 1965, "A Platform with 6 Degrees of Freedom," *Proc. of Institution of Mechanical Engineers*, 1965~1966, 180, Part 1, No. 15, pp. 371~386.

Strang, G., 1980, "Linear Algebra and Its Applications," 1st ed., Harcourt Brace Jovanovich, Publishers, San Diego.

Terano, T., Asai, K. and Sugeno, M., 1992, "Fuzzy Systems Theory and Its Applications," Academic Press, INC., Harcourt Brace Jovanovich, Publishers.

Ting, Y., Tosunoglu, S. and Tesar, D., 1993, "A Control Structure for Fault-Tolerant Operation of Robotic Manipulators," *Proc. IEEE Conf. on Robotics and Automation*, Vol. 3, pp. 684~690.

Vijaykumar, Waldron, K. J., and Tsai, M. J., 1986, "Geometric Optimization of Serial Chain Manipulator Sturctures for Walking Volume and Dexterity," *Int. Journal of Robotics Research*,

Vol. 5, No. 2.

Wood, K. L., 1989, "A Method for the Representation and Manipulation of Uncertainties in Preliminary Engineering Design," Ph.D Dissertation, Department of Mechanical Engineering, California Institute of Technology.

Wu, E., Difler, J., Hwang, J. and Chladek, J. T., 1991, "A Fault-Tolerant Joint Drive System for Space Shuttle Remote Manipulator System," *Proc IEEE Conf. on Robotics and Automation*, Vol. 3, pp. 2504~2509.

Yi, B. J., Freeman, R. A. and Tesar, D., 1992, "Force and Stiffness Transmission of Redundantrly Actuated Mechanisms : The Case for a Spherical Shoulder Mechanism," *Proc. 1992 ASME Biennial Mechanism Conf.*, Scottsdale, AZ.